Mechanistic and Electronic Insights into a Working NiAu Single-Atom Alloy Ethanol Dehydrogenation Catalyst

Georgios Giannakakis,[1] Paul Kress,[2] Kaining Duanmu,[3] Hio Tong Ngan,[3] George Yan,[3] Adam S. Hoffman,[4] Zhen Qi,[5] Antonios Trimpalis,[1] Leelavathi Annamalai,[1] Mengyao Ouyang,[1] Jilei Liu,[1] Nathaniel Eagan,[1] Juergen Biener,[5] Dimosthenis Sokaras,[4] Maria Flytzani-Stephanopoulos,[1λ] Simon R. Bare,[4*] Philippe Sautet,[3,6*] and E. Charles H. Sykes[2*]

[1]*Department of Chemical and Biological Engineering, Tufts University, 4 Colby Street, Medford, Massachusetts 02155, United States*

[2]*Department of Chemistry, Tufts University, 62 Talbot Avenue, Medford, Massachusetts 02155, United States*

[3]*Department of Chemical and Biomolecular Engineering, University of California, Los Angeles, California 90095, United States*

[4]*Stanford Synchrotron Radiation Lightsource, SLAC National Accelerator Laboratory, Menlo Park, California 94025, United States*

[5]*Nanoscale Synthesis and Characterization Laboratory, Lawrence Livermore National Laboratory, Livermore, CA 94550, United States*

[6]*Department of Chemistry and Biochemistry, University of California, Los Angeles, California 90095, United States*

[λ] Maria Flytzani-Stephanopoulos passed away on October 28th 2019

[*]Corresponding Authors: srbare@slac.stanford.edu, sautet@ucla.edu, charles.sykes@tufts.edu

Abstract

Elucidation of reaction mechanisms and the geometric and electronic structure of the active sites themselves is a challenging, yet essential task in the design of new heterogeneous catalysts. Such investigations are best implemented *via* a multi-pronged approach that comprises ambient pressure catalysis, surface science, and theory. Herein, we employ this strategy to understand the workings of NiAu single-atom alloy (SAA) catalysts for the selective non-oxidative dehydrogenation of ethanol to acetaldehyde and hydrogen. The atomic dispersion of Ni is paramount for selective ethanol to acetaldehyde conversion, and we show that even the presence of small Ni ensembles in the Au surface results in the formation of undesirable byproducts *via* C-C scission. Spectroscopic, kinetic, and theoretical investigations of the reaction mechanism reveal that both C-H and O-H bond cleavage steps are kinetically relevant and single Ni atoms are confirmed as the active sites. X-ray absorption spectroscopy studies allow us to follow the charge of the Ni atoms in the Au host before, under, and after a reaction cycle. Specifically, in the pristine state the Ni atoms carry a partial positive charge which increases upon coordination to the electronegative oxygen in ethanol and decreases upon desorption. This type of oxidation state cycling during reaction is similar to the behavior of single-site homogenous catalysts. Given the unique electronic structure of many single-site catalysts, such a combined approach in which the atomic-scale catalyst structure and charge state of the single atom dopant can be monitored as a function of its reactive environment is a key step towards developing structure function relationships that inform the design of new catalysts.

Keywords

Single-site catalysts; DFT; single-crystal studies; active site identification; HERFD-XANES

INTRODUCTION

Following Taylor's concept of the active center of a catalytic surface, identifying the sites responsible for the catalytic reactivity and selectivity of a heterogeneous catalyst is a challenging but crucial task in the rational design and development of more efficient catalysts for industrially significant reactions.[1] Towards this goal, single-site heterogeneous catalysts, with their active site homogeneity make characterization and understanding catalyst structure-function relationships achievable.[2] Within the framework of single-atom catalysis, single-atom alloys (SAAs) that comprise isolated atoms of active metals embedded in more inert but more selective metal hosts are a subclass that has drawn particular attention in recent years.[3,4] This interest arises from their unique properties that include selective reactions for a variety of chemistries, resistance to coking, and tolerance to CO poisoning, as well as their ability to escape linear scaling relationships that limit traditional catalyst performance.[5] Interestingly, in some cases it has been shown that despite being alloyed in the surface of a host metal, the minority metal atom in the SAA retains a free-atom-like electronic structure, which can account for some of the unique catalytic behavior of SAAs.[6] The origin of this effect stems from poor energetic and spatial overlap of the d-orbitals of the dopant and host metals which results in the dopant atom exhibiting a pronounced, narrow density of states near the Fermi level.

Despite the progress in investigating the electronic structure of SAAs theoretically, *operando* information on the precise state of the dopant atoms in working catalysts is still rather elusive. Identifying the electronic configuration of the active site during the reaction can yield more information about the behavior of SAA catalysts under operating conditions and help elucidate the role of the dopant metal atom in the reaction. While theoretical tools and catalytic activity tests can give indirect insights into the process, advanced spectroscopic instruments are critical for gaining a full picture of such structure-function relationships. To that end, work by Greiner et al. demonstrated the free-atom-like d-state of the minority element, Cu, in CuAg SAAs *in situ* and under methanol reforming conditions *via* ambient pressure x-ray photoemission spectroscopy (AP-XPS). Their measurements had to be performed on model unsupported CuAg catalysts, making it difficult to extrapolate to working supported catalysts under similar conditions. As XPS is not a trace elements technique it is not possible to perform similar measurements on SAA catalysts present in low concentration. Similar challenges arise for conventional x-ray absorption spectroscopy measurements rendering such investigations challenging. High-energy-resolution fluorescence detection (HERFD) x-ray absorption near edge structure spectroscopy (XANES) is a promising alternative that can circumvent these limitations. The high sensitivity of the technique allows determination of the electronic structure of even the most dilute samples under reactive atmospheres.[7] Its ability to extract high quality information on the oxidation state of the element

of interest and its interaction with reactant molecules has proven valuable in identifying the reaction mechanism on single-atom Ir on $MgAl_2O_4$ catalysts with low Ir loadings.[8]

The focus of the current work, non-oxidative ethanol dehydrogenation (EDH), is of industrial interest owing to its potential to provide a route for hydrogen and acetaldehyde production.[9] Acetaldehyde is recognized as a key building block for the production of high-added value chemicals, such as acetic acid, 1-butanol, acetate esters, C-8 aromatics, and jet fuel. Alternatives have been sought to replace the inefficient industrially used oxidative process, including reactants and products over-oxidation, and challenges and costs associated with H_2O separation.[10] The non-oxidative route can ameliorate these issues, as the selectivity to the desirable acetaldehyde remains high and the main byproduct is H_2 that does not require a costly separation process.[11,12] Given the significance of the EDH reaction, the development of active, selective, and stable catalysts is an important goal.

Copper-based catalysts have been considered commercially for this reaction due to their considerable reactivity and high selectivity to the desired pathway. Unfortunately, these catalysts suffer from rapid irreversible deactivation, observed even during the first hour on stream, due to particle sintering.[13] Au-based catalysts are a promising alternative, due to their higher sintering resistance and selectivity for the reaction.[14,15] However, selectivity comes at the expense of lower activity. As a consequence, regardless of the support used, supported gold nanoparticles (NPs) exhibit appreciable hydrogen and acetaldehyde yield only at elevated temperatures (above 200°C).[15] Alternatively, we have shown that Au NPs doped with Ni atoms can be reactive at considerably lower temperatures (below 150°C) compared to other Au-based systems, while maintaining close to 100% selectivity without deactivation over a large temperature range.[16]

A key step towards designing new catalysts is understanding and characterizing of the state of the catalyst under operating conditions and the associated reaction mechanism. While such studies of the EDH reaction mechanism have been reported on Ag-based[17,18] and Cu-based systems supported on various supports or doped with minimal amounts of more reactive metals,[19,20] investigations of Au-based systems have been limited to theoretical investigations and single-crystal studies on Pd-rich surfaces.[21–23] Herein, we provide an in-depth study of the EDH reaction mechanism on both Au and NiAu SAA catalysts, identifying Ni single atoms as the active site, and interrogating their oxidation state under reaction conditions by employing kinetic and spectroscopic investigation on supported and unsupported catalysts coupled with single-crystal studies, theoretical calculations, and x-ray techniques.

EXPERIMENTAL SECTION

Catalyst synthesis

Synthesis of supported NiAu nanoparticles was achieved following a sequential reduction method as discussed previously.[16] Briefly, PVP-Au colloids were synthesized as described by Tedsree et al.[24] at a PVP:Au molar ratio of 35:1. More specifically, ~500 mg of gold precursor

($HAuCl_4$) dissolved in 10 mL ethylene glycol was added to a solution containing 50 mL ethylene glycol and 2 g of PVP (MW=58,000 g/mol). An inert gas atmosphere was obtained by flowing N_2 or He through the flask. $NaHCO_3$ was added, and the temperature was immediately increased to 90°C and held for 2 h before cooling to ambient temperature. The wine-red color of the suspension was indicative of Au NP formation. Nickel precursor ($NiCl_2$) dissolved in ethylene glycol was then added into the suspension to obtain the desired atomic ratio of Ni and Au. Small amounts of hydrazine (1.6 mM) and an appropriate amount (10 μL/mL) of 1 M NaOH were added to promote Ni reduction[25] while the temperature was increased to 60°C and held for 1 h before the mixture was cooled to room temperature. The fumed silica support was first calcined in static air at 650°C for 5 h to remove organic impurities and then suspended in ethanol (1 g pre-calcined silica per 100 mL ethanol). The mixture was thoroughly mixed with 2 h of stirring and 1 h of sonication before the NiAu solution was added dropwise while the slurry remained under sonication. The resulting solution containing $NiAu/SiO_2$ was kept stirring overnight. After filtration and washing with ethanol and DI water, the final sample was dried under vacuum overnight and calcined in air at 400°C for 5 h to remove the capping ligand (PVP) and improve the association of the metal and the support. The Au metal loading on the silica support is 5%, as indicated by inductively coupled plasma (ICP) elemental analysis, while the average particle size of these NiAu nanoparticles is 12 ± 2 nm, as has been shown previously with transmission electron microscopy.[16] Synthesis of small (~8 nm in size) Ni nanoparticles supported on silica was performed following the steps described above for the decoration of Au nanoparticles with Ni atoms by reducing Ni precursor in the presence of small amounts of hydrazine.[25]

Synthesis of unsupported nanoporous NiAu samples was performed at the Lawrence Livermore National Laboratory, as described previously.[16] Briefly, nanoporous Au was first fabricated by immersing a silver-gold alloy (Ag_{70} Au_{30}) in concentrated HNO_3 solution to selectively leach silver from the Ag-Au alloy over a two-day period. Wet impregnation of the resulting nanoporous Au with nickel(II) nitrate hexahydrate solution then ensured the filling of the pores with the desired amount of Ni precursor. The sample was subsequently freeze dried and annealed at 500°C for 1 h under hydrogen in order to reduce the deposited Ni[26] and decompose the salt.[27]

Catalyst characterization

Diffuse reflectance infrared Fourier transform spectroscopy (DRIFTS) measurements were conducted on a Thermo Scientific Nicolet iS50 FTIR Spectrometer with a Praying Mantis high temperature reaction chamber. Samples were reduced *in situ* with 10% H_2/He at a flow rate of 10 mL/min at 350°C for 1 h. Ethanol was introduced in the DRIFTS cell via a saturator kept at room temperature, and He was used as a carrier gas.

High-resolution transmission electron microscopy (HR-TEM) images and energy-dispersive x-ray spectroscopy (EDXS) measurements were obtained using a JEOL 2010 electron microscope (200kV and 107 μA). An ethanol solution of the supported NPs was prepared and drop casted on a carbon film over a copper microgrid for imaging.

High energy fluorescence detection (HERFD) XANES measurements were collected at Beamline 6-2 at SSRL. A liquid-nitrogen-cooled double-crystal Si(311) monochromator was equipped to select the energy of the incident beam with a flux of ~$3 \cdot 10^{12}$ photons$\cdot s^{-1}$. A Rowland circle spectrometer (radius 1 m) equipped with three spherically bent Si(800) analyzers and a silicon drift detector were used to select the Ni K-β1 (8264.66 eV) emission line with a measured energy resolution of 1.3 eV. A nickel foil standard was scanned in the transmission mode for energy calibration. Nine consecutive scans were collected for each sample to improve the signal-to-noise ratio. The analysis of the HERFD XANES data was carried out with the software ATHENA of the IFEFFIT package.[28] The Ni K-edge (determined by the first inflection point of the absorption edge of the Ni foil) was calibrated to align absolute energy in the HERFD XANES spectra using a known glitch in the monochromator observed in the I0 signal of each scan. A least-squares Gaussian fit of the glitch, determined the error in the energy calibration of the samples to be 22 meV/0.022 eV. Energy calibration was achieved by aligning the glitch in each scan to the glitch in the Ni foil reference scans.

Ambient pressure reactor studies

The ambient pressure reaction studies were performed in a fixed-bed continuous flow reactor in which the catalyst was diluted at a 1:5 ratio with pre-calcined sand and stabilized between two quartz wool plugs. The reactor was heated by a furnace equipped with a temperature controller connected to a K-type thermocouple positioned at the top of the catalyst bed. Prior to testing, all catalysts were reduced under a flow of H_2 (20% in He) with a flow rate of 10 mL/min at 400°C for 2 h to reduce NiO to metallic Ni[26,29]. The typical reaction gas composition was 2% ethanol (Sigma Aldrich, 200 proof) in He (99.999%, Airgas), achieved by feeding ethanol *via* a syringe pump into a flow of He controlled by a mass flow controller at a total flow rate of 20 mL/min unless otherwise stated. Kinetic isotope effect experiments were conducted using ethanol-OD (CH_3CH_2OD; Sigma Aldrich, 99% atom D) and ethanol-1,1-d_2 (CH_3CD_2OH; Sigma Aldrich, 98% atom D). Reactant and product concentrations were measured by gas chromatography (Agilent 7890B). A flame ionization detector was used for the detection of ethanol, acetaldehyde, and ethyl acetate, which were separated on an HP-PLOT Q capillary column. H_2, CO, and CO_2 were separated on a Carboxen-1000 packed column and detected using a thermal conductivity detector.

Particular attention was paid to ensure operation away from equilibrium (~1% conversion) during the kinetic isotope effect (KIE) experiments, while the equilibrium conversion at the conditions tested stands at 50% (at 150℃ for NiAu) and 80% (at 220℃ for Au). Reactor results are expressed as ethanol consumption rate, as the only products under these conditions are acetaldehyde and hydrogen and the carbon balance is nearly 100%.

Computational details

The single-atom alloy surface was modeled by using a 3×3 unit cell. The PBE functional with dDsC dispersion correction, 400 eV cut-off energy and 7×7×1 K-points were used.[30,31] All the calculations were performed with *VASP*.[32,33] The reaction rate constant k_{TST} was calculated from the thermodynamic formulation of transition state theory (TST):

$$k_{\mathrm{TST}} = \frac{k_B \mathrm{T}}{h} \mathrm{e}^{-\frac{\Delta \mathrm{G}^{\neq}}{\mathrm{RT}}} \quad (1)$$

Where $\Delta G^{\neq}$ is the free energy difference between transition state and initial state ($G_{TS} - G_{IS}$).

Translational, rotational, and vibrational degrees of freedom were included in the free energy calculations for the gaseous species. Eq. (2) and Eq. (3) were used to obtain the free energy values for linear and non-linear gaseous molecules, respectively:

$$G = E_{DFT} + ZPE + 3.5k_BT + \sum \frac{\epsilon_i}{exp\left(\frac{\epsilon_i}{k_BT} - 1\right)} - T(S_{trans} + S_{rot} + S_{vib}) \quad (2)$$

$$G = E_{DFT} + ZPE + 4k_BT + \sum \frac{\epsilon_i}{exp\left(\frac{\epsilon_i}{k_BT} - 1\right)} - T(S_{trans} + S_{rot} + S_{vib}) \quad (3)$$

where E_{DFT} is the electronic energy given by DFT, ZPE is the zero-point energy, k_B is the Boltzmann constant, T is the temperature, ϵ_i is the harmonic energy and S is the entropy.

Surface species were assumed to have lost the translational and rotational degrees of freedom. Their free energies were hence calculated as follows:

$$G = E_{DFT} + ZPE + \sum \frac{\epsilon_i}{exp\left(\frac{\epsilon_i}{k_BT} - 1\right)} - TS_{vib} \quad (4)$$

Single crystal studies

Temperature-programmed desorption (TPD) analysis was performed in a ultra-high vacuum chamber (base pressure $<1\text{x}10^{-10}$ mbar) using a Au(111) single crystal cleaned by cycles of sputtering Ar^+ (1.5 keV, 10 μA) followed by 720 K anneals.[34] Cleanliness was monitored *via* x-ray photoelectron spectroscopy. Ni was deposited onto the crystal held at 380 K using a physical vapor deposition source (EFM 3, Focus GmbH) at a flux of 0.04 ML/min as verified by CO

titrations. The TPD traces were recorded using a heating rate of 2 K/s and the desorbing species monitored with a quadrupole mass spectrometer (HAL 301, Hiden Analytical).

Reflection absorption infrared spectroscopy (RAIRS) experiments were performed at the Center for Functional Nanomaterials (CFN) at Brookhaven National Laboratory in a UHV system with a connected preparation chamber and x-ray photoelectron spectroscopy (XPS) chamber for measurement of the Ni and cleanliness of sample. XPS data were obtained at room temperature using a SPECS PHOIBOS NAP 150 hemispherical analyzer and a monochromatic Al Kα x-ray source (1486.6 eV, ~0.25eV linewidth) focused on the sample to a spot size <300 μm (0.5 eV step, 0.1 s dwell time, 5 scans, 50 pass energy). Infrared data were collected using a Bruker 80 V spectrometer with a polarizer and an MCT detector (2000 scans, 4 cm^{-1} resolution). The sample was placed in a UHV chamber with KBr windows and the surface set at ~8° to the beam. The RAIR spectra were taken at room temperature while the chamber was filled to 1 x 10^{-6} mbar with CO.

RESULTS AND DISCUSSION

Significance of reactive atom dilution - Single-crystal and theoretical studies

As a first step in investigating structure-function relationships in NiAu alloys, UHV and theoretical studies of model NiAu(111) crystal surfaces were employed. Figure 1A shows temperature program desorption (TPD) profiles of hydrogen (m/z = 2) evolution after ethanol deposition on a NiAu(111) surface as a function of Ni coverage. At low Ni coverages (< 0.15 monolayer (ML)), two H_2 desorption peaks are observed, at 140 and 175 K. These desorption peaks are attributed to ethanol, which does not react with Au(111) under these UHV conditions (Fig. 1D) but rather desorbs below 200 K at low Ni coverages (Fig. 1B) and contributes intensity to the m/z = 2 mass spec signal. At higher Ni coverages (0.21 ML), two m/z = 2 peaks that we can attribute to H_2(g) appear at higher temperatures (280 and 356 K) and are associated with complete decomposition of ethanol. Importantly, no acetaldehyde was seen desorbing at any Ni coverage. To probe the nature of the Ni sites in the Au surface, and thus relate surface structure to chemical reactivity, CO RAIRS was performed on the NiAu SAA and the 0.22 ML NiAu surface. The 0.22 ML NiAu surface contains Ni ensembles as evidenced by the appearance of bridge bound CO at 1911 cm^{-1}, while the 0.03 ML NiAu surface only had one IR peak corresponding to CO atop Ni atoms at 2034 cm^{-1} (Fig. 1C).[35,36] It should be noted that similar changes in the IR spectra were observed when comparing NiAu nanoparticles of varying Ni content that result in samples comprising solely Ni isolated atoms or a mixture of isolated Ni atoms and small ensembles (Fig. S2). Coupled with the TPD results, our observations reveal that under UHV conditions, single atoms of Ni in Au adsorb ethanol reversibly without activation. On the contrary, higher Ni coverages lead to the formation of small Ni ensembles which catalyze the unselective decomposition of ethanol as evidenced by the evolution of high temperature H_2 (Fig. 1D).[37,38]

This high sensitivity of the ethanol dehydrogenation reaction towards the decomposition pathway in the presence of Ni ensembles is further understood *via* DFT calculations of the

acetaldehyde decomposition barrier (i.e., C-C bond cleavage) over Ni monomer, dimer, and trimer sites (Table 1). While the C-C bond decomposition barrier is 2.04 eV for the NiAu SAA surface (denoted as Ni_1Au in Table 1), a significant ~0.9 eV drop is observed for Ni dimers (Ni_2Au), and trimers (barrier of 1.16 and 0.97 eV respectively). This is consistent with the easy C-C bond cleavage which has been reported for Pt-group metals (PGM) that coordinate acetaldehyde in a η^2(C,O) conformation[39] facilitating the decomposition pathway. As a result, in the presence of even small ensembles of Ni, acetaldehyde decomposition towards CO_x, CH_4, and H_2 is observed.[16] On the other hand, isolation of the active Ni atoms in the Au lattice prevents this adsorption mode, and instead the acetaldehyde molecule is bound to the SAA surface *via* a η^1(O)-conformation (as shown later in Fig. 3B), which leads to its reversible adsorption/desorption as observed in the TPD experiments.

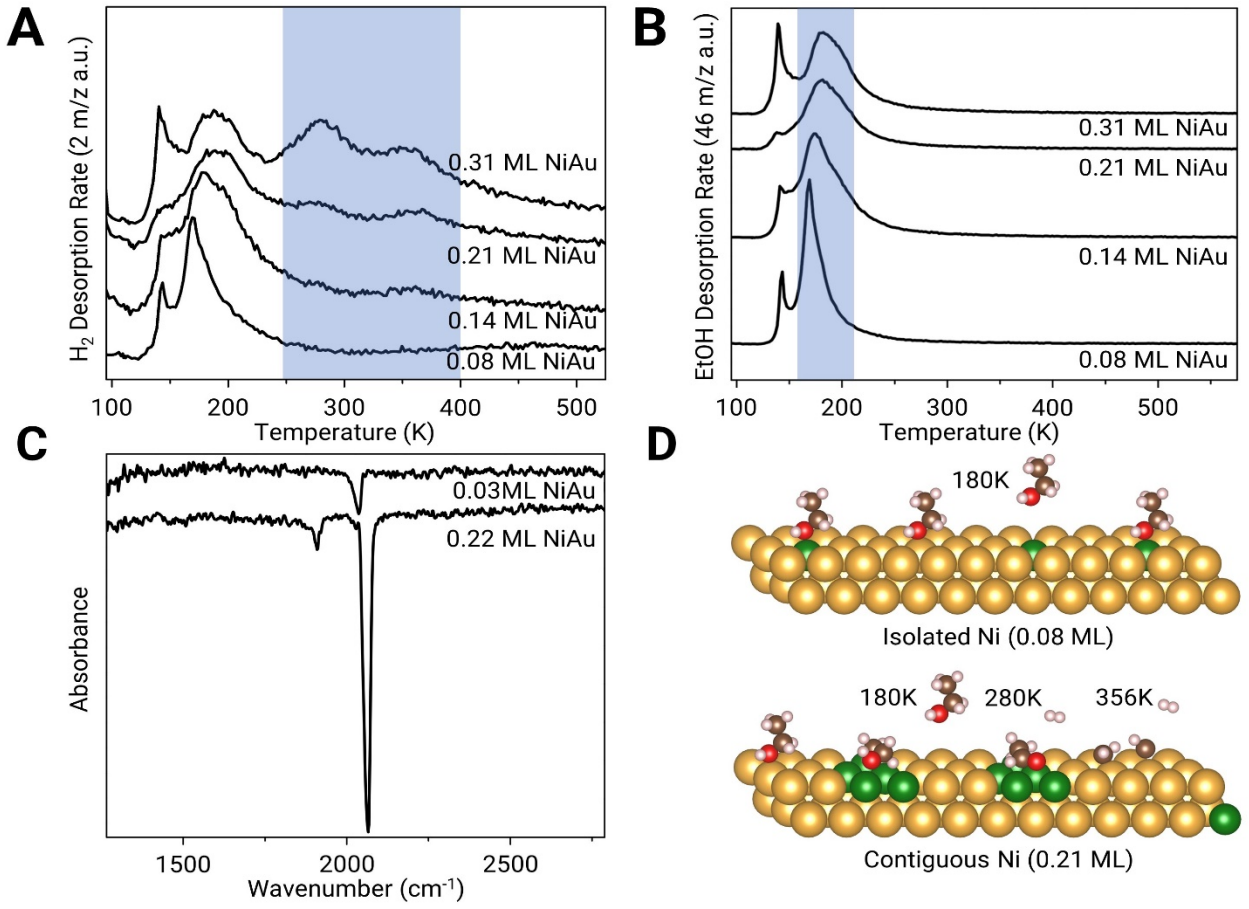

Figure 1. *Temperature Programmed Desorption traces after ethanol exposure for* ***A)*** *H_2 (m/z = 2). The shaded rectangle highlights the temperature window over which H_2 desorption from ethanol decomposition occurs and* ***B)*** *Ethanol (m/z = 46) from NiAu(111) as a function of Ni coverage. The shaded rectangle highlights the temperature window over which the reversible desorption of ethanol occurs.* ***C)*** *CO-RAIRS of 0.03 ML and 0.22 ML Ni coverages* ***D)*** *Scheme of*

ethanol interaction with NiAu(111) surfaces presenting different Ni ensembles (upper: Isolated Ni atoms; lower: extended Ni surfaces)

Table 1. Calculated C-C bond scission barriers for Ni_x-Au(111) surfaces x=1,2,3

(111) surface	C-C bond scission, eV
Ni_1Au	2.04
Ni_2Au	1.16
Ni_3Au	0.97

Reaction Mechanism – Experimental studies

Our surface science and DFT studies indicated that the presence of even small Ni ensembles leads to unfavorable reactivity in terms of unselective ethanol decomposition on Ni ensembles. This indicates that dilute NiAu samples with IR signals characteristic of CO atop single Ni atoms and a lack of bridge bound IR signals at lower wavenumber should be the most promising catalysts for the selective conversion of ethanol to acetaldehyde and hydrogen. The first consideration when moving from unsupported single crystal model systems to practical nanoparticle catalysts is the effect of the support. While it is known that silica is inactive for ethanol decomposition at temperatures below 300℃[40], one must ensure that no Ni is deposited on the support as catalyst reactivity could be incorrectly assigned to Ni in a SAA as opposed to small cluster form. First, imaging of the silica supported NiAu SAA samples *via* EDXS elemental mapping showed no measurable signal of Ni deposition on the silica support. Ni is only detected where the Au NPs reside (Fig. S1), as expected for the sequential reduction synthesis method, which involves Ni (75 ppm) addition to Au colloids and synthesis of the colloidal NiAu nanoparticles in the solution prior to deposition on the silica support.[16] The lack of Ni on the support and the coordination of Ni only with Au maximizes the possibility for site uniformity, an essential requirement for the kinetic and spectroscopic investigations that follow.

Operando ethanol DRIFTS investigations were first employed to deduce the reaction mechanism, as has been previously performed on Ag- and Cu- based catalysts.[17,19] Comparison of the ethanol DRIFT spectra between Au/SiO_2 and $NiAu/SiO_2$ shows clear evidence for the beneficial effect of Ni atom doping on the reactivity, as acetaldehyde was found to be formed on the surface of NiAu at temperatures below 150℃(Fig. 2B), while signs of acetaldehyde formation on Au/SiO_2 were not observed until 200℃(Fig. 2A). Formation of acetaldehyde either bound on the surface or present in the gas phase can be verified by the peaks observed at 1730 and 1760 cm^{-1}, respectively.[41] These results are in line with our previous reactor tests in which we compared NiAu to pure Au nanoparticle catalysts and find that Ni atoms make Au active at lower temperatures while maintaining 100% selectivity to acetaldehyde. Specifically, a considerable drop in the apparent activation energy was measured (96±5 kJ/mol for Au vs 61±2 kJ/mol for

NiAu), while NiAu catalysts demonstrated 100% selectivity at 27% conversion at 250℃ for more than 50 hours on stream.[16] Unfortunately, DRIFTS studies were inconclusive towards determining the reaction mechanism for the supported NiAu/SiO_2 catalysts of this study, as spectator ethoxy species adsorbed on the silica interfere with interpretation of the intermediates, as discussed in the Supporting Information (Fig. S3).

In KIE studies of silica supported Au NPs and NiAu SAAs, the catalytic activity of non-deuterated ethanol was compared to isotopically labeled ethanol, deuterated in either the α C-H or O-H position. First, the activity of non-deuterated ethanol over an Au/SiO_2 catalyst was followed under steady state at 220℃ at conditions away from equilibrium. The acetaldehyde formation rate was measured as 8.7 μmol/mol_{Au}·s (Fig 2C). Following that, deuterated ethanol (CH_3CD_2OH) was introduced to the flow reactor and a two-fold decrease in catalytic activity was observed. Experiments over silica supported NiAu SAAs conducted at 150℃ (Fig. 2D) showed a similar drop in the reactivity (k_H/k_D= 1.9), signifying the presence of a KIE linked with the C-H bond cleavage elementary step.[42–44] This is in line with the existing literature on alcohol activation over various bimetallic systems.[19] However, further investigation on the role of the O-H dissociation step in the reaction mechanism is required. To that end, deuterated ethanol was used, where the hydrogen atom in the O-H is replaced by a deuterium atom (CH_3CH_2OD). A drop in reactivity is observed for both NiAu SAAs and Au NPs (~ 1.5 in both cases, Fig, 2C, D) when switching between the regular (OH) and deuterated (OD) ethanol in the feed, indicating that the O-H bond cleavage step also plays a kinetically relevant role in the reaction mechanism. This is also consistent with previous work in which the kinetic significance of both C-H and O-H bond scission steps has been discussed for the non-oxidative activation of ethanol and 2-octanol over Cu and Ni catalysts supported on acidic or basic supports.[20,45]

Related to these results, Suskevich et al. obtained similar data from their spectroscopic and isotopic experiments for the EDH reaction over Ag/SiO_2 catalysts (k_H/k_D=1.9 and 1.8 for C-H and O-H respectively).[17] Their analysis suggested the existence of a concerted mechanism in which O-H activation takes place on the support and C-H activation occurs on the Ag surface, and they concluded that the two sites must be in close proximity. As mentioned above, ethoxy species formed on the support are in fact spectator species in the reaction and do not react further. However, while there is a possibility for a concerted, two-site mechanism over supported monometallic Au, it is unlikely that this mechanism also holds for the case of NiAu SAAs. First, migration of the ethoxy species from the support to NiAu domains is unlikely and second, as the Ni atoms are present in very low concentration, it is not expected that a sufficient number exist in close enough proximity to SiO_2 to activate ethanol. However, while this analysis is challenging for supported NiAu SAA nanoparticles we also studied unsupported nanoporous NiAu SAAs in order to deconvolute the role of the SAA from that of the support. Our KIE investigations of the unsupported catalysts yielded similar values (Fig. S4) to the supported catalysts (k_H/k_D=1.7 and 1.5 for C-H and O-H respectively), suggesting that the reaction mechanism is the same in both silica supported and unsupported nanoporous catalysts. This claim can be further supported by the

similar apparent activation energy measured on nanoporous (np-) NiAu and NiAu/SiO_2, as shown previously.[16] These results allow us to rule out that the aforementioned concerted EDH reaction, involving sites on both the support and the NiAu SAA nanoparticles, is the primary mechanism.

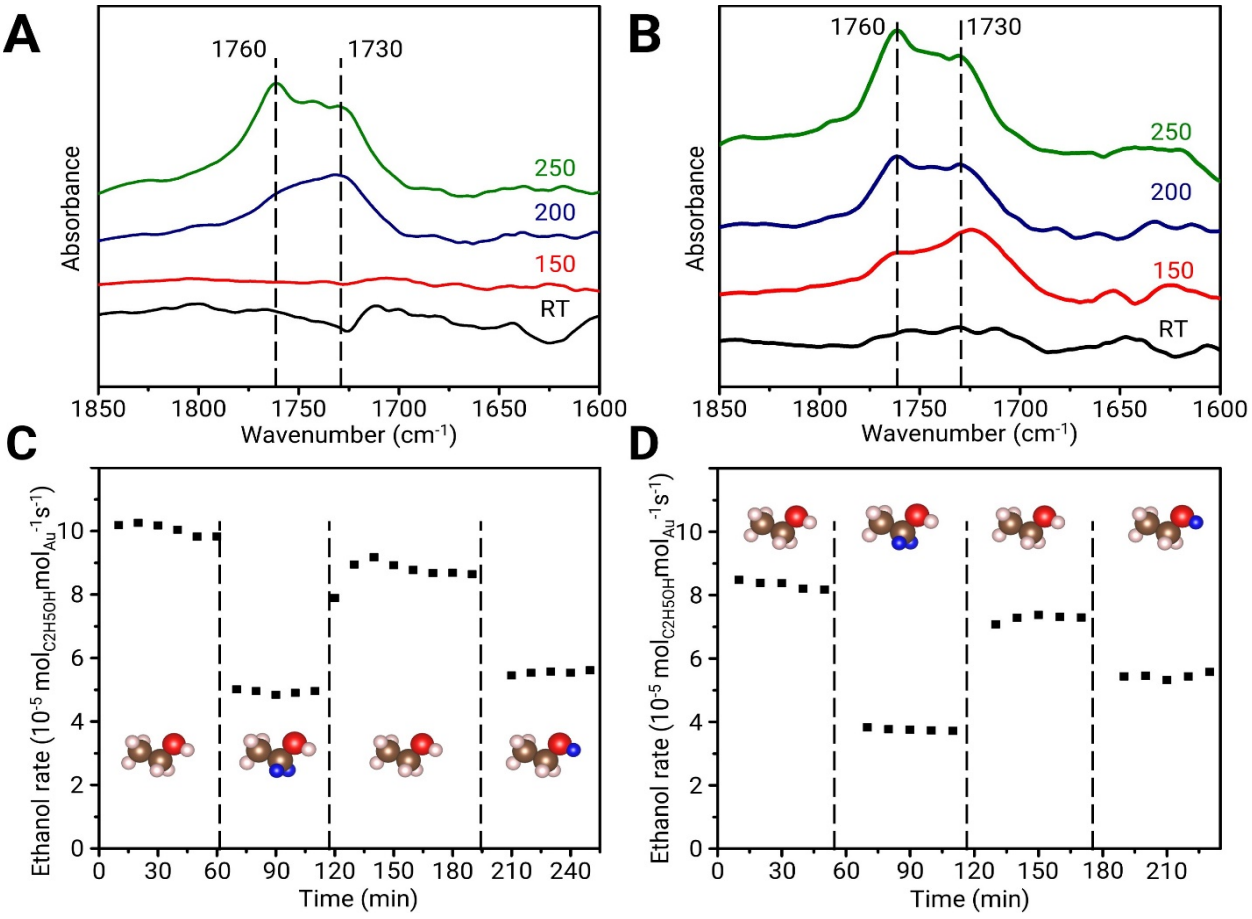

Figure 2. *Ethanol DRIFTS using* ***A)*** *Au/SiO_2 and* ***B)*** *$Ni_{0.005}Au/SiO_2$ focusing on the C-O regime (1850-1600 cm^{-1}). KIE studies using* ***C)*** *Au/SiO_2 (2 kPa EtOH in He, 10 cc/min, 150 mg catalyst, 220℃, ethanol injected: i) pure ethanol, ii) CH_3CH_2OD, iii) pure ethanol, iv) CH_3CD_2OH and* ***D)*** *$NiAu/SiO_2$ (2 kPa EtOH in He, 20c c/min, 150 mg catalyst, 180 ℃, ethanol injected: i) pure ethanol ii) CH_3CD_2OH, iii) pure ethanol iv) CH_3CH_2OD*

Reaction mechanism - Theoretical studies

The KIE results provide insights into the kinetic significance of the C-H and O-H cleavage steps, and we further this understanding through DFT simulations of the reaction mechanism. H_2 partial pressures equal to those measured at the reactor outlet (0.0003 bar) at the temperature examined in kinetic tests (150℃) were used for the calculations and the pressure of aldehyde was set to the same value for stoichiometric reasons. The internal adsorption energy of ethanol on Ni is significant (-0.66 eV), but at high temperature and low pressure, the entropy of gas phase ethanol is large, which makes the initial adsorption state endergonic. The free energy profile for the dehydrogenation of CH_3CH_2OH on a NiAu(111) SAA surface is shown in Figure 3A, and two possible reaction pathways are calculated: α C-H dissociation followed by O-H dissociation (blue

pathway) and O-H dissociation followed by α C-H dissociation (red pathway), as shown in Fig. 3B. After the first dehydrogenation step (TS1), the dehydrogenated H atoms are able to desorb from the alloy surface (IM1 to IM2) because the gas phase H_2 is thermodynamically more stable than surface bound H and the barriers for the translation and recombination of H atoms and desorption of H_2 from the alloy surface are quite low. Based on the overall barriers, it is evident that the pathway initiated by the C-H dissociation (blue) is the more favorable one. While there is a general consensus in literature studies of supported catalysts that O-H bond activation is the first step, followed by C-H bond scission, here we observe a different pathway in line with DFT and microkinetic modelling studies of EDH on Pd(111) and Pt(111).[46,47] This reaction pathway was also suggested for unsupported NiCu alloys[48], however on pure Ni(111), O-H activation has been identified as the first step.[38]

On the blue pathway, the effective free energy activation barrier, also called energetic span,[49] is between the initial gas state of ethanol (0 eV) and the OH bond cleavage transition state (TS2, 1.17 eV). This effective free energy barrier, which controls the rate of the dehydrogenation reaction, can be viewed as the sum of the reaction free energy of the first C-H cleavage step, from gas phase to the IM2 intermediate, and the free energy barrier of the second O-H cleavage step. The corresponding enthalpy barrier (Fig. S5) is 0.73 eV, in good agreement with the experimental value (0.59 eV).

Under the reaction conditions in our study (**Figure 3a**), the energetic span approximation can capture the important features of the reaction mechanism. The predicted rates agree with those found by a microkinetic model parameterized with DFT-calculated kinetic coefficients (**Tables S1 and S2**). This agreement can be explained by the degree of rate control (DRC) of surface intermediates and transition states (**Table S3**). Out of all surface intermediates, only the bare active site has appreciable DRC (-0.996). Correspondingly, it is clear from **Figure 3a** that the formation of all other reactive intermediates is endergonic with respect to the gases in the reaction environment. On the other hand, the transition state for the dehydrogenation of the 1,1-hydroxyethyl intermediate has the highest degree of rate control out of all TS (0.943, **Table S3**). In combination with the tendency for the DRC of all TS in such a single-net-gas-reaction mechanism to add up to 1, we see that the energetic span approximation is suitable for the interpretations of reactivity in our case where adsorbate coverage is small.[50] As we have now identified the rate-controlling states in the reaction mechanism, the KIE can be qualitatively addressed by comparing the Gibbs free energy spans of the dehydrogenation (and de-deuteration) of CH_3CH_2OH, CH_3CD_2OH and CH_3CH_2OD.[51]

To link with the KIE experiments, H-D isotope exchange effects were calculated and the dehydrogenation free energy profiles for CH_3CD_2OH and CH_3CH_2OD on the NiAu(111) SAA surface are given in the SI (Fig. 6 and Fig. 7, respectively). Both isotope exchange result in an increase of the energetic span, in line with the observed decreased rate. For the C-H/C-D exchange, the reaction free energy of the C-H bond cleavage first step is increased (less favorable) mainly from the smaller zero-point energy of the C-D bond, while the activation barrier of the O-H bond

is unchanged. For the O-H/OD exchange, the O-D activation energy is increased. Hence the calculations suggest that the decreased rates from isotopic exchange stem from different reason, and do not necessary imply that both C-H and O-H activations have a large degree of rate control. In the calculated blue profile, only O-H activation has a large degree of rate control, but isotope exchange at the C-H bond also shows a KIE effect. The energy difference between C-H and O-H cleavage transition states on the blue profile (0.1 eV) is however too small (considering approximations in the calculation) to definitively exclude that C-H bond cleavage has a degree of rate control in the dehydrogenation reaction.

Our DFT simulation of the EDH reaction on Au(111) (Fig. S10) shows that the first dehydrogenation step (TS1) is the rate determining step and the blue reaction pathway still has a lower overall barrier (1.84 eV) than the red reaction pathway (2.05 eV), which means that the reaction is very slow, as opposed to NiAu(111) SAA, and the optimal reaction pathway occurs *via* α C-H dissociation followed by O-H dissociation on Au. The DFT calculations also demonstrate that the reaction barriers for EDH are much higher on pure Au (Fig. S11) than on NiAu SAA (enthalpic barrier of 0.94 eV for Au vs. 0.73 eV for NiAu), in qualitative agreement with experimental enthalpy barriers (0.96 eV vs 0.59 eV).[16] Most importantly, the NiAu SAA does not over bind ethanol, as is the case for pure Ni, and therefore regardless of whether the O-H or C-H bond is broken first, the reaction mechanisms on the SAA are selective to the preferred acetaldehyde and hydrogen products.

Selective poisoning supports the Ni atom active site model – single crystal and reactor studies

Our combined spectroscopic, kinetic, and theoretical investigations have shed light on the preferred EDH reaction pathways on both Au and NiAu SAAs. We also demonstrated with DFT (Fig. 3A) that both kinetically relevant reaction steps (C-H and O-H cleavage) take place over the Ni atom, pointing at isolated Ni atom sites in Au being the active site of the catalyst. Related to this, it is noteworthy that active site identification on the same SAA catalyst in oxidative coupling reactions show $[Au\text{-}O_x]^-$ species as the active site.[52] Therefore, to further solidify our hypothesis that individual, isolated Ni atoms are the active sites for the non-oxidative EDH reaction, reactor tests with a poison that selectively blocks only the Ni sites were employed. Specifically, CO is known to bind strongly to group 10 metals but not to coinage metals. DFT calculations by Darby et al. put the CO desorption temperature from the NiAu (111) SAA surface at 340 K.[53] In contrast, DFT and experimental measurements indicate that CO desorbs from Au(111) below 100 K.[54] CO TPD from single crystal NiAu(111) surfaces of various Ni coverages were studied under UHV (Fig. 3C). Desorption of CO from low concentrations of Ni was observed at 325 K, in close agreement with the theoretical calculations. For Ni coverages >0.2 ML a secondary desorption feature at lower temperature is observed in the CO TPD spectra (highlighted in red in Fig. 3C), consistent with the formation of Ni aggregate/Au interfaces.[34] Comparing the desorption temperature of CO and ethanol (Fig. 1B), it is clear that desorption of CO takes place at considerably higher temperatures than ethanol (325 vs 190 K), indicating that CO should outcompete ethanol for binding to the Ni atom sites.[55,56] Guided by these surface science and

theoretical results, ambient pressure reactor tests were performed on supported NiAu SAAs where the Ni site was poisoned with CO (Fig 3D). First, ethanol was introduced into the reactor and the ethanol consumption rate measured, followed by co-flowing carbon monoxide and ethanol through the reactor. A considerable drop (~70%) in the catalytic activity was noticed in the presence of CO, due to the CO binding to Ni more strongly than ethanol essentially poisoning Ni sites, as was predicted from the surface science results. As a result, the only active sites available to ethanol are Au sites. Importantly, the ~4-fold lower ethanol consumption rate on CO-poisoned NiAu SAAs matches the ethanol consumption rate on pure Au NPs at those conditions (Fig. 2D). This provides definitive evidence that the isolated Ni atom sites are involved in the active site for the EDH reaction. Furthermore, once the flow of CO is halted, the NiAu SAA catalyst activity returns to previously measured levels, consistent with the reversible adsorption/desorption of CO observed in the single crystal measurements.

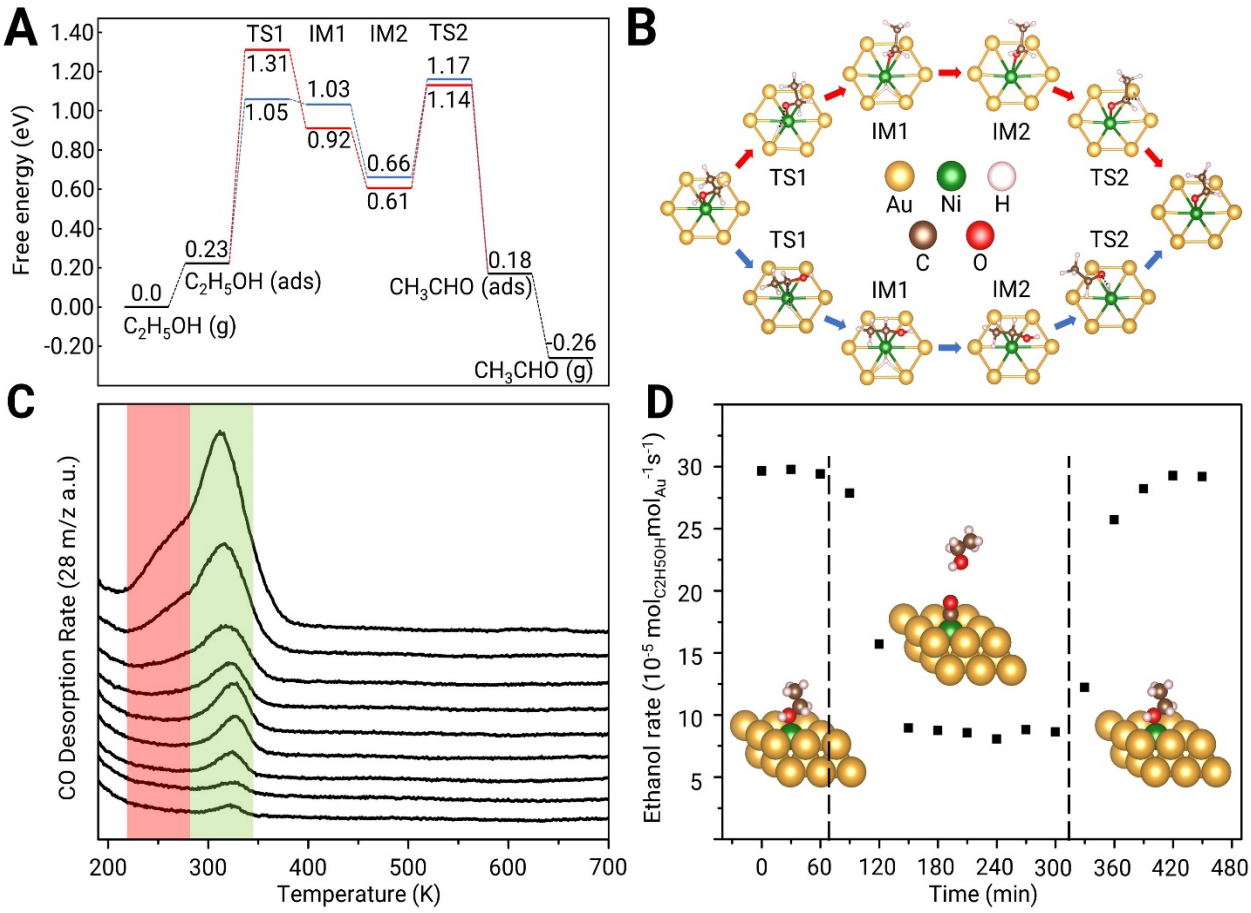

Figure 3. A) *Free energy diagram of ethanol dehydrogenation on the NiAu(111) SAA surface. The conditions used for the construction are: $P(H_2)$ = 0.0003bar, $P(C_2H_5OH)$ = 0.02 bar, $P(CH_3CHO)$ = 0.0003bar, and T = 423.15K.* ***B)*** *Adsorption configurations, visualized using VESTA.*[57] ***C)*** *Temperature Programmed Desorption profile for CO desorption from NiAu(111) at various Ni coverages (0.01 ML to 0.61 ML).* ***D)*** *Ethanol dehydrogenation tests at 473 K under i) 2kPa ethanol, ii) 2kPa ethanol & 2kPa CO and iii) 2kPa ethanol balanced in He.*

To further support the claims about the effect of CO on reactivity, DFT simulations in which a CO molecule was bound to the Ni atom were performed and the reaction pathway computed (Fig. S12). Expectedly, the energetics of the pathway match that of the bare Au(111) surface (Fig. S10), and only the Au atoms neighboring the Ni atom exhibit very small shift in their d-band center (Fig. S13). It should be noted however that according to our DFT results, the ethanol molecule binds more favorably to the next available Au atom, possibly due to steric repulsion from the CO molecule (Fig. S12). The above theoretical results, when coupled with the reactor tests that were guided by the single crystal experiments, constitute solid evidence that the individual, isolated Ni atoms are the active sites for the EDH reaction.

***Operando* interrogation of dopant metal atoms - HERFD XANES**

Having identified Ni atoms as the active sites responsible for the remarkable EDH performance of NiAu SAA catalysts, we probed the electronic structure of Ni atom active sites under reaction conditions and their interaction with the reactant, ethanol. Specifically, HERFD XANES has the potential to provide more detailed information than conventional XANES[58,59] and has been recently reported to be useful for understanding heterogeneous catalysts in terms of quantifying charge redistribution effects in ionic liquid-coated single-atoms of Ir, and a correlation to the reactivity of those catalysts for butadiene hydrogenation was developed.[60] Herein, HERFD XANES spectra were collected on fresh and reduced supported nanoparticle catalysts as well as those under ethanol flow at between RT and 150℃ and at 200℃. The fresh catalyst HERFD XANES spectrum exhibits characteristic features of a Ni^{2+} state, including the signature pre-edge feature at 8,332.0 eV, which is the formally dipole-forbidden 1s → 3d transition that gains intensity from being quadrupole-allowed, as well as due to hybridization with O p-states.[61] After catalyst reduction to a metallic state under H_2 at 400℃ and purging under He, this pre-edge feature disappeared, and a shift in edge position and the drop of the white line intensity are consistent with the Ni atoms being reduced (blue line in Fig. 4). Notably, when the NiAu SAA sample is in its metallic reduced state the charge on the Ni atoms is not zero but rather slightly positive, as demonstrated by comparing to the HERFD XANES spectrum of small, reduced Ni NPs (black line in Fig. 4). This result is in agreement with our DFT Bader charge analysis that yielded a charge equal to +0.33 on the Ni atom (Table S4). This result is of particular significance since the traditional view of metals and alloys would suggest that metal atoms in a metallic alloy should not carry a charge. However, the positive charging on the Ni atoms is consistent with the difference in electronegativity between Ni (1.91) and Au (2.54). Related to this, previous normal XANES analyses of other Ni-based (NiCu, NiIr) SAAs concluded that Ni atoms in those cases were present in the metallic state.[19,62] While it is possible that no shift in edge position or drop of the white line intensity occurs in NiCu or NiIr SAAs and that Ni atoms exist in a neutral state in these cases due to the lower electronegativity of Cu (1.90), it is more probable that such shifts were not visible with conventional XANES. On the contrary, our HERFD XANES data taken on the reduced catalyst suggests that Ni atoms in NiAu SAAs carry a positive charge arising from charge transfer with the Au metal host, in agreement with our DFT results.

By way of context, XPS is the traditional method for determining the electronic charge of the sites of a catalytic surface by correlating binding energy shifts to electron transfer between the different elements of an alloy. For example, Rodriguez and Goodman followed charge redistribution in various metals in single-crystal studies *via* XPS and determined the direction of the electron density flow in a metal-metal bond.[63] Similarly, investigations by Geitner et al. employed synchrotron XPS and XANES to study unsupported CuAg SAAs and reported that Cu atoms isolated in Ag had a local negative charge.[6] However, the XPS approach becomes impossible for supported dilute alloy catalysts in which the dopant concentration is <1% as XPS is not a trace element technique (~100ppm in the case of $NiAu/SiO_2$ SAA), a concentration regime at which HERFD XANES can still operate reliably. Similar evidence of the electronic structure modulation of Ni by the presence of another metal, has been demonstrated by DeBeer and co-workers in Ni_3Co_1 alloys, as evidenced *via* HERFD XANES analysis, as well as by the Bao group on Ni_1Pt_4 alloys based on conventional XANES measurements, however in both cases considerably higher concentrations of Ni were present in the samples.[64,65]

While little experimental data exists for charge transfer in SAAs, the electronic structure of Ni atoms in NiAu SAAs has been examined theoretically.[66] Specifically, the d-states of Ni atoms in a Au(111) host was computed by Thirumalai and Kitchin and their results revealed a very narrow electronic state near the Fermi level indicative of a lack of hybridization of the Ni d-states with the host Au. In fact, these computed Ni atom d-states resembled those of a free Ni atom in a vacuum, the so-called "free atom like state".[6] In Kitchin's work, it was demonstrated that these free-atom-like states are rather common in SAAs and most prominent for Ag- and Au-based SAAs compared to Cu-based ones. These free atom like states have been experimentally demonstrated for CuAg SAAs.[6] Specifically, Greiner *et al.* used *in situ* XPS studies of CuAg SAAs to demonstrate that the lack of hybridization of Ag and Cu leads to a pronounced free atom like state at the Cu atom and they related this to the system's ability to perform methanol steam reforming reaction with a lower barrier. Our DFT calculations (Fig. S14) show that the d-states of the Ni atom in Au are indeed unperturbed by the Au coordinating atoms both in the presence and in the absence of the reactant, demonstrating a free atom like d state.

In terms of chemical reactivity, one would intuitively expect that the local positive charge of Ni atom should interact with the electron dense lone pair of the oxygen atom of ethanol.[67] Indeed, upon introduction of ethanol into the reactor, the Ni absorption edge shifts slightly to higher energy (green line in Fig. 4) indicative of slight positive charging of the Ni upon ethanol adsorption. Our own DFT calculations which show that ethanol (denoted as C_2H_5OH(ads) in Fig. 3a) binds to the Ni atom through the oxygen atom is consistent with this picture. Furthermore, Bader charge analysis on the Ni atom binding the ethanol molecule *via* the O atom shows a local charge of +0.44 on the Ni atom (Table S4), increased compared to the bare surface (+0.33), in agreement with the HERFD XANES spectrum. These HERFD XANES features indicate the charged Ni site are persistent at temperatures up to 150℃. At temperatures above 150℃ ethanol conversion to acetaldehyde and hydrogen begins, and by 200℃(grey line in Fig. 4) the Ni edge has shifted almost

entirely to its position prior to reaction (blue line in Fig. 4). The result denotes a reduced coordination of ethanol to the Ni atom, as expected based on the lower surface coverage of ethanol on the surface at these elevated temperatures. Overall, these results indicate that a redox process is taking place on the Ni atom; ethanol partially oxidizes it, while at higher temperatures the Ni atoms return to a more reduced state. This behavior provides further evidence for Ni atoms as the active sites which adsorb and selectively convert ethanol to acetaldehyde and hydrogen.

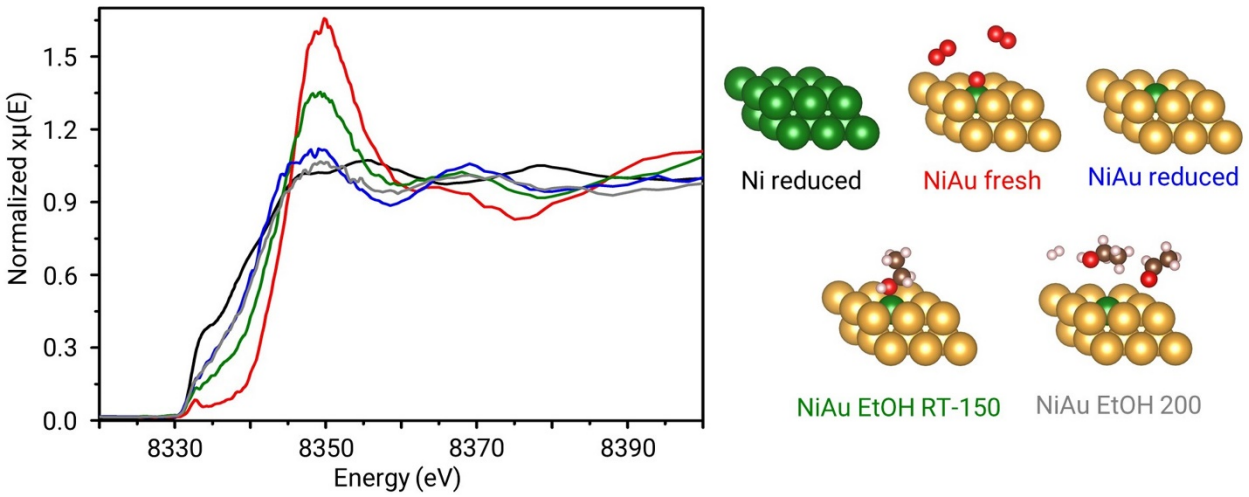

Figure 4. *HERFD XANES spectra of reduced Ni/SiO_2 (black), as-prepared NiAu/SiO_2 (red), reduced NiAu/SiO_2 (blue), NiAu/SiO_2 under ethanol from RT to 150℃ (green), and NiAu/SiO_2 under ethanol at 200℃ (grey).*

Taken together, the combined theoretical, single-crystal, and nanoparticles studies were critical in obtaining a deep understanding of the NiAu SAA system and showcasing how it can be used for the design of new catalysts. The single-crystal and theoretical studies are in full agreement with previous NiAu/SiO_2 SAA CO IR data[16] in terms of the importance of maintaining very high levels of dilution, such that the Ni atoms are always isolated from one another in the host matrix. This result demonstrates how ethanol can be used as a probe molecule for the characterization of active site ensemble sizes in bimetallic catalytic surfaces. Alloy particles with high dispersion of the reactive metal atoms should only yield acetaldehyde and hydrogen under EDH reaction conditions. On the contrary, evidence of undesirable product formation from the decomposition pathway indicates formation of reactive metal aggregates in the surface of the inert host. Similar experimental and theoretical reports for NiCu and PdAu dilute alloys bolster this argument.[23,68,69] Therefore, the EDH reaction has the potential to serve as a probe reaction for the surface characterization of dilute alloys and complement other characterization techniques as is the case for ethylene hydrogenation which has been shown to be a probe of the metallic surface area of Pt-based catalysts.[70]

Furthermore, the three-pronged approach was shown to be capable of outlining the reaction mechanism and identifying the active sites for the reaction. This is especially highlighted by the KIE studies, supported by DFT calculations, as well as the active site identification by controlled

poisoning of the Ni sites. These examples underline the powerful complementary nature of single atom alloys, which allows for their accurate modelling towards understanding their properties and designing new catalysts based on theoretical insights.[71] Furthermore, SAA catalysts can be promising candidates for facilitating industrially the non-oxidative ethanol dehydrogenation process, as they combine high reactivity, while maintaining the host-like selectivity (~100%) and stability over a broad range of operating conditions without the addition of toxic oxides (Table S5).

Last, interrogating of the electronic structure of SAAs *via* high resolution spectroscopic tools can help shed light not only on the redox nature of the reaction mechanism of a given reaction but also pave the way for the rational design of optimal catalysts. This approach of using partial charges to inform on reaction mechanisms has been used very successfully for many years in organic chemistry.[72] Related to heterogeneous catalysis, Upham et al. showed theoretically that the less negative charge on Ni atoms dispersed in molten metals (Bi, Pb, Sn), the higher its reactivity for direct conversion of methane to hydrogen.[73] Similar relationships can potentially be established for more systems and bond activation steps, leading to a toolbox that can help guide the choice of the most promising catalysts for selective transformations. Coupling this information on the electronic structure of the dopant atoms with extensive screening of promising SAAs for the activation of important small molecules, as demonstrated by Darby et al. would considerably advance this understanding.[5,74] We showcase here that HERFD XANES is a valuable tool for these ultra-dilute alloy systems that are challenging to investigate with conventional XANES and XPS experiments.

CONCLUSIONS

Herein we have used a multipronged surface science, theory, and practical catalysis approach to characterize the geometric and electronic structure of the active sites of a working NiAu SAA nanoparticle catalyst as well as the reaction mechanism. Specifically, site isolated Ni atoms in Au nanoparticles are shown to be active and 100% selective for the low temperature conversion of ethanol to acetaldehyde and hydrogen. We demonstrate via isotopic experiments on a working catalyst that both O-H and C-H cleavage steps impact the reaction rate and elucidate the reaction pathway with theory, validated by a clear agreement on the effective enthalpy barrier between experiment and theory. Our calculations indicate that the preferred pathway on the NiAu(111) SAA surface starts by the C-H bond cleavage, the second O-H bond scission step being rate controlling. The effective free energy barrier is the sum of the reaction energy of the fist C-H step and the activation barrier of the second O-H step, so that C-H/C-D exchange also decreases the reaction rate even if its transition state does not have a strong degree of rate control. Our calculations hence imply that measuring a KIE effect on two consecutive reaction steps does not imply that both transition states have a large degree of rate control. Guided by our surface science experiments we use preferential adsorption of CO at the Ni atom active sites to show that the NiAu SAA catalyst reactivity is decreased to the same level as pure Au when CO is present in the reactant

flow, thus demonstrating that the Ni atoms are the active sites. Furthermore, we use HERFD XANES to follow the charge state of the dilute Ni atoms under reaction conditions and demonstrate that, in agreement with theory, Ni atoms cycle their charge state during reaction in a manner akin to homogeneous catalysts. Given that acetaldehyde is produced industrially via an inefficient oxidative process in which water must be separated from acetaldehyde, supported SAA NiAu nanoparticle catalysts offer great promise for the production of pure acetaldehyde and the value-added byproduct hydrogen.

Supporting Information

Details of microkinetic simulations, STEM, IR, and KIE catalyst characterization studies, DFT calculated energetic profiles and density of states, Bader charges, and catalyst reference data.

Acknowledgments
This work was supported as part of the Integrated Mesoscale Architectures for Sustainable Catalysis, an Energy Frontier Research Center funded by the U.S. Department of Energy, Office of Science, Basic Energy Sciences under award no. DE-SC0012573. Co-ACCESS, is supported by the U.S. Department of Energy, Office of Basic Energy Sciences, Chemical Sciences, Geosciences and Biosciences. Use of the Stanford Synchrotron Radiation Lightsource, SLAC National Accelerator Laboratory, is supported by the U.S. Department of Energy, Office of Science, Office of Basic Energy Sciences under Contract No. DE-AC02-76SF00515. DFT calculations were performed on the Hoffman2 cluster at the UCLA Institute for Digital Research and Education (IDRE) and the National Energy Research Scientific Computing Center (NERSC) of the U.S. Department of Energy. Work at Lawrence Livermore National Laboratory (LLNL) was performed under the auspices of the US Department of Energy by LLNL under contract DE-AC52-07NA27344.

References

(1) Taylor, H. S. A Theory of the Catalytic Surface. *J. Phys. Chem.* **1925**, *28* (1), 105–111.

(2) Kaiser, S. K.; Chen, Z.; Faust Akl, D.; Mitchell, S.; Pérez-Ramírez, J. Single-Atom Catalysts across the Periodic Table. *Chem. Rev.* **2020**, *120* (21), 11703–11809. https://doi.org/10.1021/acs.chemrev.0c00576.

(3) Hannagan, R. T.; Giannakakis, G.; Flytzani-Stephanopoulos, M.; Sykes, E. C. H. Single-Atom Alloy Catalysis. *Chem. Rev.* **2020**, *120* (21), 12044–12088. https://doi.org/10.1021/acs.chemrev.0c00078.

(4) Giannakakis, G.; Flytzani-Stephanopoulos, M.; Sykes, E. C. H. Single-Atom Alloys as a Reductionist Approach to the Rational Design of Heterogeneous Catalysts. *Acc. Chem. Res.* **2019**, *52* (1), 237–247. https://doi.org/10.1021/acs.accounts.8b00490.

(5) Darby, M. T.; Stamatakis, M.; Michaelides, A.; Sykes, E. C. H. Lonely Atoms with

Special Gifts: Breaking Linear Scaling Relationships in Heterogeneous Catalysis with Single-Atom Alloys. *J. Phys. Chem. Lett.* **2018**, *9* (18), 5636–5646. https://doi.org/10.1021/acs.jpclett.8b01888.

(6) Greiner, M. T.; Jones, T. E.; Beeg, S.; Zwiener, L.; Scherzer, M.; Girgsdies, F.; Piccinin, S.; Armbrüster, M.; Knop-Gericke, A.; Schlögl, R. Free-Atom-like d States in Single-Atom Alloy Catalysts. *Nat. Chem.* **2018**, *10* (10), 1008–1015. https://doi.org/10.1038/s41557-018-0125-5.

(7) Hoffman, A. S.; Sokaras, D.; Zhang, S.; Debefve, L. M.; Fang, C. Y.; Gallo, A.; Kroll, T.; Dixon, D. A.; Bare, S. R.; Gates, B. C. High-Energy-Resolution X-Ray Absorption Spectroscopy for Identification of Reactive Surface Species on Supported Single-Site Iridium Catalysts. *Chem. - A Eur. J.* **2017**, *23* (59), 14760–14768. https://doi.org/10.1002/chem.201701459.

(8) Lu, Y.; Wang, J.; Yu, L.; Kovarik, L.; Zhang, X.; Hoffman, A. S.; Gallo, A.; Bare, S. R.; Sokaras, D.; Kroll, T.; Dagle, V.; Xin, H.; Karim, A. M. Identification of the Active Complex for CO Oxidation over Single-Atom Ir-on-MgAl 2 O 4 Catalysts. *Nat. Catal.* **2019**, *2* (2), 149–156. https://doi.org/10.1038/s41929-018-0192-4.

(9) Sun, J.; Wang, Y. Recent Advances in Catalytic Conversion of Ethanol to Chemicals. *ACS Catal.* **2014**, *4* (4), 1078–1090. https://doi.org/10.1021/cs4011343.

(10) Mitsudome, T.; Mikami, Y.; Funai, H.; Mizugaki, T.; Jitsukawa, K.; Kaneda, K. Oxidant-Free Alcohol Dehydrogenation Using a Reusable Hydrotalcite-Supported Silver Nanoparticle Catalyst. *Angew. Chemie* **2008**, *120* (1), 144–147. https://doi.org/10.1002/ange.200703161.

(11) Eagan, N. M.; Kumbhalkar, M. D.; Buchanan, J. S.; Dumesic, J. A.; Huber, G. W. Chemistries and Processes for the Conversion of Ethanol into Middle-Distillate Fuels. *Nat. Rev. Chem.* **2019**, *3* (4), 223–249. https://doi.org/10.1038/s41570-019-0084-4.

(12) Eckert, M.; Fleischmann, G.; Jira, R.; Bolt, H. M.; Golka, K. Acetaldehyde. In *Ullmann's Encyclopedia of Industrial Chemistry*; 2011. https://doi.org/10.1002/14356007.a01.

(13) Tu, Y. J.; Chen, Y. W. Effects of Alkaline-Earth Oxide Additives on Silica-Supported Copper Catalysts in Ethanol Dehydrogenation. *Ind. Eng. Chem. Res.* **1998**, *37* (7), 2618–2622. https://doi.org/10.1021/ie9708135.

(14) Guan, Y.; Hensen, E. J. M. Ethanol Dehydrogenation by Gold Catalysts: The Effect of the Gold Particle Size and the Presence of Oxygen. *Appl. Catal. A Gen.* **2009**, *361* (1–2), 49–56. https://doi.org/10.1016/j.apcata.2009.03.033.

(15) Gazsi, A.; Koós, A.; Bánsági, T.; Solymosi, F. Adsorption and Decomposition of Ethanol on Supported Au Catalysts. *Catal. Today* **2011**, *160* (1), 70–78. https://doi.org/10.1016/j.cattod.2010.05.007.

(16) Giannakakis, G.; Trimpalis, A.; Shan, J.; Qi, Z.; Cao, S.; Liu, J.; Ye, J.; Biener, J.; Flytzani-Stephanopoulos, M. NiAu Single Atom Alloys for the Non-Oxidative

Dehydrogenation of Ethanol to Acetaldehyde and Hydrogen. *Top. Catal.* **2018**, *61* (5–6), 475–486. https://doi.org/10.1007/s11244-017-0883-0.

(17) Sushkevich, V. L.; Ivanova, I. I.; Taarning, E. Mechanistic Study of Ethanol Dehydrogenation over Silica-Supported Silver. *ChemCatChem* **2013**, *5* (8), 2367–2373. https://doi.org/10.1002/cctc.201300033.

(18) Sushkevich, V. L.; Ivanova, I. I. Mechanistic Study of Ethanol Conversion into Butadiene over Silver Promoted Zirconia Catalysts. *Appl. Catal. B Environ.* **2017**, *215*, 36–49. https://doi.org/10.1016/j.apcatb.2017.05.060.

(19) Shan, J.; Liu, J.; Li, M.; Lustig, S.; Lee, S.; Flytzani-Stephanopoulos, M. NiCu Single Atom Alloys Catalyze the C-H Bond Activation in the Selective Non-Oxidative Ethanol Dehydrogenation Reaction. *Appl. Catal. B Environ.* **2017**, *226* (December 2017), 534–543. https://doi.org/10.1016/j.apcatb.2017.12.059.

(20) Hanukovich, S.; Dang, A.; Christopher, P. Influence of Metal Oxide Support Acid Sites on Cu-Catalyzed Nonoxidative Dehydrogenation of Ethanol to Acetaldehyde. *ACS Catal.* **2019**, *9* (4), 3537–3550. https://doi.org/10.1021/acscatal.8b05075.

(21) Evans, E. J.; Li, H.; Yu, W. Y.; Mullen, G. M.; Henkelman, G.; Mullins, C. B. Mechanistic Insights on Ethanol Dehydrogenation on Pd-Au Model Catalysts: A Combined Experimental and DFT Study. *Phys. Chem. Chem. Phys.* **2017**, *19* (45), 30578–30589. https://doi.org/10.1039/c7cp05097f.

(22) Li, H.; Henkelman, G. Dehydrogenation Selectivity of Ethanol on Close-Packed Transition Metal Surfaces: A Computational Study of Monometallic, Pd/Au, and Rh/Au Catalysts. *J. Phys. Chem. C* **2017**, *121* (49), 27504–27510. https://doi.org/10.1021/acs.jpcc.7b09953.

(23) Li, H.; Evans, E. J.; Mullins, C. B.; Henkelman, G. Ethanol Decomposition on Pd-Au Alloy Catalysts. *J. Phys. Chem. C* **2018**, *122* (38), 22024–22032. https://doi.org/10.1021/acs.jpcc.8b08150.

(24) Tedsree, K.; Li, T.; Jones, S.; Chan, C. W. A.; Yu, K. M. K.; Bagot, P. A. J.; Marquis, E. A.; Smith, G. D. W.; Tsang, S. C. E. Hydrogen Production from Formic Acid Decomposition at Room Temperature Using a Ag–Pd Core–Shell Nanocatalyst. *Nat. Nanotechnol.* **2011**, *6* (5), 302–307. https://doi.org/10.1038/nnano.2011.42.

(25) Wu, S. H.; Chen, D. H. Synthesis and Characterization of Nickel Nanoparticles by Hydrazine Reduction in Ethylene Glycol. *J. Colloid Interface Sci.* **2003**, *259* (2), 282–286. https://doi.org/10.1016/S0021-9797(02)00135-2.

(26) Rodriguez, J. A.; Hanson, J. C.; Frenkel, A. I.; Kim, J. Y.; Pérez, M. Experimental and Theoretical Studies on the Reaction of H_2 with NiO: Role of O Vacancies and Mechanism for Oxide Reduction. *J. Am. Chem. Soc.* **2002**, *124* (2), 346–354. https://doi.org/10.1021/ja0121080.

(27) Elmasry, M. A. A.; Gaber, A.; Khater, E. M. H. Thermal Decomposition of Ni(II) and

Fe(III) Nitrates and Their Mixture. *Journal of Thermal Analysis and Calorimetry*. 1998, pp 489–495. https://doi.org/10.1023/A:1010155203247.

(28) Ravel, B.; Newville, M. ATHENA, ARTEMIS, HEPHAESTUS: Data Analysis for X-Ray Absorption Spectroscopy Using IFEFFIT. *J. Synchrotron Radiat.* **2005**, *12* (4), 537–541. https://doi.org/10.1107/S0909049505012719.

(29) Ma, L.; Jia, I.; Guo, X.; Xiang, L. High Performance of Pd Catalysts on Bimodal Mesopore for the Silica Catalytic Oxidation of Toluene. *Chinese J. Catal.* **2014**, *35* (0), 108–119. https://doi.org/10.1016/S1872.

(30) Steinmann, S. N.; Corminboeuf, C. Comprehensive Benchmarking of a Density-Dependent Dispersion Correction. *J. Chem. Theory Comput.* **2011**, *7* (11), 3567–3577. https://doi.org/10.1021/ct200602x.

(31) Perdew, J. P.; Burke, K.; Ernzerhof, M. Generalized Gradient Approximation Made Simple. *Phys. Rev. Lett.* **1996**, *77* (18), 3865–3868. https://doi.org/10.1103/PhysRevLett.77.3865.

(32) Kresse, G.; Hafner, J. Ab Initio Molecular-Dynamics Simulation of the Liquid-Metalamorphous- Semiconductor Transition in Germanium. *Phys. Rev. B* **1994**, *49* (20), 14251–14269. https://doi.org/10.1103/PhysRevB.49.14251.

(33) Kresse, G.; Hafner, J. Ab Initio Molecular Dynamics for Liquid Metals. *Phys. Rev. B* **1993**, *47* (1), 558–561. https://doi.org/10.1103/PhysRevB.47.558.

(34) Wang, Z.-T.; Darby, M. T.; Therrien, A. J.; El-Soda, M.; Michaelides, A.; Stamatakis, M.; Sykes, E. C. H. Preparation, Structure, and Surface Chemistry of Ni–Au Single Atom Alloys. *J. Phys. Chem. C* **2016**, *120* (25), 13574–13580. https://doi.org/10.1021/acs.jpcc.6b03473.

(35) Xu, C.; Koel, B. E. Influence of Alloyed Sn Atoms on the Chemisorption Properties of Ni(111) as Probed by RAIRS and TPD Studies of CO Adsorption. *Surf. Sci.* **1995**, *327* (1–2), 38–46. https://doi.org/10.1016/0039-6028(94)00816-7.

(36) Vasquez, N.; Muscat, A.; Madix, R. J. The Effect of Site Distribution on Desorption Kinetics: Carbon Monoxide from Ni(100). *Surf. Sci.* **1994**, *301* (1–3), 83–88. https://doi.org/10.1016/0039-6028(94)91289-0.

(37) Kratochwil, T.; Wittmann, M.; Küppers, J. Adsorption of Ethanol on Ni(100) Surfaces. *J. Electron Spectros. Relat. Phenomena* **1993**, *64–65* (C), 609–617. https://doi.org/10.1016/0368-2048(93)80128-9.

(38) Gates, S. M.; Russell, J. N.; Yates, J. T. Bond Activation Sequence Observed in the Chemisorption and Surface Reaction of Ethanol on Ni(111). *Surf. Sci.* **1986**, *171* (1), 111–134. https://doi.org/10.1016/0039-6028(86)90565-0.

(39) Mavrikakis, M.; Barteau, M. A. Oxygenate Reaction Pathways on Transition Metal Surfaces. *J. Mol. Catal. A Chem.* **1998**, *131* (1–3), 135–147. https://doi.org/10.1016/S1381-1169(97)00261-6.

(40) Matsumura, Y.; Hashimoto, K.; Yoshida, S. Selective Dehydrogenation of Ethanol over Dehydrated Silica. *J. Catal.* **1989**, *117* (20), 135–143. https://doi.org/10.1039/C39870001599.

(41) Demri, D.; Hindermann, J.; Diagne, C.; Kiennemann, A. Oxygenates on Rhodium-Containing Catalysts during CO + H_2 Reactions. *J. Chem. Soc. - Faraday Trans.* **1994**, *90* (3), 501–506.

(42) Campbell, C. T. Finding the Rate-Determining Step in a Mechanism: Comparing DeDonder Relations with the "Degree of Rate Control." *J. Catal.* **2001**, *204* (2), 520–524. https://doi.org/10.1006/jcat.2001.3396.

(43) Campbell, C. T. Future Directions and Industrial Perspectives Micro- and Macro-Kinetics: Their Relationship in Heterogeneous Catalysis. *Top. Catal.* **1994**, *1* (3–4), 353–366. https://doi.org/10.1007/BF01492288.

(44) Chen, K.; Iglesia, E.; Bell, A. T. Kinetic Isotopic Effects in Oxidative Dehydrogenation of Propane on Vanadium Oxide Catalysts. *J. Catal.* **2000**, *192* (1), 197–203. https://doi.org/10.1006/jcat.2000.2832.

(45) Chen, H.; He, S.; Xu, M.; Wei, M.; Evans, D. G.; Duan, X. Promoted Synergic Catalysis between Metal Ni and Acid-Base Sites toward Oxidant-Free Dehydrogenation of Alcohols. *ACS Catal.* **2017**, *7* (4), 2735–2743. https://doi.org/10.1021/acscatal.6b03494.

(46) Li, M.; Guo, W.; Jiangs, R.; Zhao, L.; Shan, H. Decomposition of Ethanol on Pd(111): A Density Functional Theory Stutdy. *Langmuir* **2010**, *26* (3), 1879–1888. https://doi.org/10.1021/la902641t.

(47) Sutton, J. E.; Panagiotopoulou, P.; Verykios, X. E.; Vlachos, D. G. Combined DFT, Microkinetic, and Experimental Study of Ethanol Steam Reforming on Pt. *J. Phys. Chem. C* **2013**, *117* (9), 4691–4706. https://doi.org/10.1021/jp312593u.

(48) Kumar, A.; Ashok, A.; Bhosale, R. R.; Saleh, M. A. H.; Almomani, F. A.; Al-Marri, M.; Khader, M. M.; Tarlochan, F. In Situ DRIFTS Studies on Cu, Ni and CuNi Catalysts for Ethanol Decomposition Reaction. *Catal. Letters* **2016**, *146* (4), 778–787. https://doi.org/10.1007/s10562-016-1706-9.

(49) Kozuch, S.; Shaik, S. How to Conceptualize Catalytic Cycles? The Energetic Span Model. *Acc. Chem. Res.* **2011**, *44* (2), 101–110. https://doi.org/10.1021/ar1000956.

(50) Campbell, C. T. The Degree of Rate Control: A Powerful Tool for Catalysis Research. *ACS Catalysis*. 2017, pp 2770–2779. https://doi.org/10.1021/acscatal.7b00115.

(51) Mao, Z.; Campbell, C. T. Kinetic Isotope Effects: Interpretation and Prediction Using Degrees of Rate Control. *ACS Catal.* **2020**, *10* (7), 4181–4192. https://doi.org/10.1021/acscatal.9b05637.

(52) Trimpalis, A.; Giannakakis, G.; Cao, S.; Flytzani-Stephanopoulos, M. NiAu Single Atom Alloys for the Selective Oxidation of Methacrolein with Methanol to Methyl Methacrylate. *Catal. Today* **2020**, *355* (April), 804–814.

https://doi.org/10.1016/j.cattod.2019.04.021.

(53) Darby, M. T.; Sykes, E. C. H.; Michaelides, A.; Stamatakis, M. Carbon Monoxide Poisoning Resistance and Structural Stability of Single Atom Alloys. *Top. Catal.* **2018**, *61* (5–6), 428–438. https://doi.org/10.1007/s11244-017-0882-1.

(54) Outka, D. A.; Madix, R. J. The Oxidation of Carbon Monoxide on the Au(110) Surface. *Surf. Sci.* **1987**, *179* (2–3), 351–360. https://doi.org/10.1016/0039-6028(87)90062-8.

(55) Marcinkowski, M. D.; Jewell, A. D.; Stamatakis, M.; Boucher, M. B.; Lewis, E. A.; Murphy, C. J.; Kyriakou, G.; Sykes, E. C. H. Controlling a Spillover Pathway with the Molecular Cork Effect. *Nat. Mater.* **2013**, *12* (6), 523–528. https://doi.org/10.1038/nmat3620.

(56) Lucci, F. R.; Darby, M. T.; Mattera, M. F. G.; Ivimey, C. J.; Therrien, A. J.; Michaelides, A.; Stamatakis, M.; Sykes, E. C. H. Controlling Hydrogen Activation, Spillover, and Desorption with Pd-Au Single-Atom Alloys. *J. Phys. Chem. Lett.* **2016**, *7* (3), 480–485. https://doi.org/10.1021/acs.jpclett.5b02400.

(57) Momma, K.; Izumi, F. VESTA 3 for Three-Dimensional Visualization of Crystal, Volumetric and Morphology Data. *J. Appl. Crystallogr.* **2011**, *44* (6), 1272–1276. https://doi.org/10.1107/S0021889811038970.

(58) Leng, Y. Vibrational Spectroscopy for Molecular Analysis. In *Materials Characterization*; 2013; pp 283–332. https://doi.org/10.1002/9783527670772.ch9.

(59) Bauer, M. HERFD-XAS and Valence-to-Core-XES: New Tools to Push the Limits in Research with Hard X-Rays? *Phys. Chem. Chem. Phys.* **2014**, *16* (27), 13827–13837. https://doi.org/10.1039/c4cp00904e.

(60) Babucci, M.; Fang, C. Y.; Hoffman, A. S.; Bare, S. R.; Gates, B. C.; Uzun, A. Tuning the Selectivity of Single-Site Supported Metal Catalysts with Ionic Liquids. *ACS Catal.* **2017**, *7* (10), 6969–6972. https://doi.org/10.1021/acscatal.7b02429.

(61) Pickering, I. J.; George, G. N.; Lewandowski, J. T.; Jacobson, A. J. Nickel K-Edge X-Ray Absorption Fine Structure of Lithium Nickel Oxides. *J. Am. Chem. Soc.* **1993**, *115* (10), 4137–4144. https://doi.org/10.1021/ja00063a035.

(62) Bai, J. qi; Tamura, M.; Nakagawa, Y.; Tomishige, K. A Nickel-Iridium Alloy as an Efficient Heterogeneous Catalyst for Hydrogenation of Olefins. *Chem. Commun.* **2019**, *55* (71), 10519–10522. https://doi.org/10.1039/c9cc04822g.

(63) Rodriguez, J. A.; Goodman, D. W. The Nature of the Metal-Metal Bond in Bimetallic Surfaces. *Science* **1992**, *257* (5072), 897–903. https://doi.org/10.1126/science.257.5072.897.

(64) Beheshti Askari, A.; Al Samarai, M.; Hiraoka, N.; Ishii, H.; Tillmann, L.; Muhler, M.; Debeer, S. In Situ X-Ray Emission and High-Resolution X-Ray Absorption Spectroscopy Applied to Ni-Based Bimetallic Dry Methane Reforming Catalysts. *Nanoscale* **2020**, *12* (28), 15185–15192. https://doi.org/10.1039/d0nr01960g.

(65) Mu, R.; Fu, Q.; Xu, H.; Zhang, H.; Huang, Y.; Jiang, Z.; Zhang, S.; Tan, D.; Bao, X. Synergetic Effect of Surface and Subsurface Ni Species at Pt-Ni Bimetallic Catalysts for CO Oxidation. *J. Am. Chem. Soc.* **2011**, *133* (6), 1978–1986. https://doi.org/10.1021/ja109483a.

(66) Thirumalai, H.; Kitchin, J. R. Investigating the Reactivity of Single Atom Alloys Using Density Functional Theory. *Top. Catal.* **2018**, *61* (5–6), 462–474. https://doi.org/10.1007/s11244-018-0899-0.

(67) Kakekhani, A.; Roling, L. T.; Kulkarni, A.; Latimer, A. A.; Abroshan, H.; Schumann, J.; Aljama, H.; Siahrostami, S.; Ismail-Beigi, S.; Abild-Pedersen, F.; Nørskov, J. K. Nature of Lone-Pair-Surface Bonds and Their Scaling Relations. *Inorg. Chem.* **2018**, *57* (12), 7222–7238. https://doi.org/10.1021/acs.inorgchem.8b00902.

(68) Shan, J.; Janvelyan, N.; Li, H.; Liu, J.; Egle, T. M.; Ye, J.; Biener, M. M.; Biener, J.; Friend, C. M.; Flytzani-Stephanopoulos, M. Selective Non-Oxidative Dehydrogenation of Ethanol to Acetaldehyde and Hydrogen on Highly Dilute NiCu Alloys. *Appl. Catal. B Environ.* **2017**, *205*, 541–550. https://doi.org/10.1016/j.apcatb.2016.12.045.

(69) Ouyang, M.; Papanikolaou, K. G.; Boubnov, A.; Hoffman, A. S.; Giannakakis, G.; Bare, S. R.; Stamatakis, M.; Flytzani-stephanopoulos, M.; Sykes, E. C. H. Directing Reaction Pathways via in Situ Control of Active Site Geometries in PdAu Single-Atom Alloy Catalysts. *Nat. Commun.* **2021**, *12* (1549), 1–11. https://doi.org/10.1038/s41467-021-21555-z.

(70) Kuhn, J. N.; Tsung, C. K.; Huang, W.; Somorjai, G. A. Effect of Organic Capping Layers over Monodisperse Platinum Nanoparticles upon Activity for Ethylene Hydrogenation and Carbon Monoxide Oxidation. *J. Catal.* **2009**, *265* (2), 209–215. https://doi.org/10.1016/j.jcat.2009.05.001.

(71) Hannagan, R. T.; Giannakakis, G.; Réocreux, R.; Schumann, J.; Finzel, J.; Wang, Y.; Michaelides, A.; Deshlahra, P.; Christopher, P.; Flytzani-Stephanopoulos, M.; Stamatakis, M.; Sykes, E. C. H. First-Principles Design of a Single-Atom–Alloy Propane Dehydrogenation Catalyst. *Science* **2021**, *372* (6549), 1444–1447.

(72) Biffis, A.; Centomo, P.; Del Zotto, A.; Zecca, M. Pd Metal Catalysts for Cross-Couplings and Related Reactions in the 21st Century: A Critical Review. *Chem. Rev.* **2018**, *118* (4), 2249–2295. https://doi.org/10.1021/acs.chemrev.7b00443.

(73) Upham, D. C.; Agarwal, V.; Khechfe, A.; Snodgrass, Z. R.; Gordon, M. J.; Metiu, H.; Mcfarland, E. W. Catalytic Molten Metals for the Direct Conversion of Methane to Hydrogen and Separable Carbon. *Science* **2017**, *921* (November), 917–921. https://doi.org/10.1126/science.aao5023.

(74) Darby, M. T.; Réocreux, R.; Sykes, E. C. H.; Michaelides, A.; Stamatakis, M. Elucidating the Stability and Reactivity of Surface Intermediates on Single-Atom Alloy Catalysts. *ACS Catal.* **2018**, *8* (6), 5038–5050. https://doi.org/10.1021/acscatal.8b00881.

TOC Graphic:

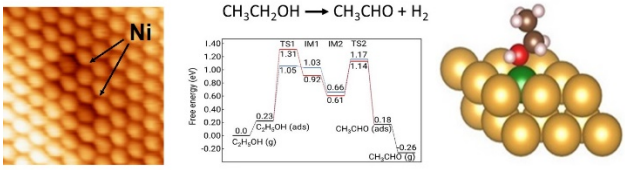
Ni
CH3CH2OH → CH3CHO + H2
Free energy (eV)
TS1
IM1
IM2
TS2
1.31
1.05
1.03
0.92
0.66
0.61
1.17
1.14
0.23
0.0
C2H5OH (ads)
C2H5OH (g)
CH3CHO (ads)
0.18
-0.26
CH3CHO (g)